Supplementary Figures

Plk1 Inhibitors and Abiraterone Synergistically Disrupt Mitosis and Kill Cancer Cells of Disparate Origin Independently of Androgen Receptor Signaling

Jesse C. Patterson, Andreas Varkaris, Peter J. P. Croucher, Maya Ridinger, Susan Dalrymple, Mannan Nouri, Fang Xie, Shohreh Varmeh, Oliver Jonas, Matthew A. Whitman, Sen Chen, Saleh Rashed, Lovemore Makusha, Jun Luo, John T. Isaacs, Mark G. Erlander, David J. Einstein, Steven P. Balk, and Michael B. Yaffe

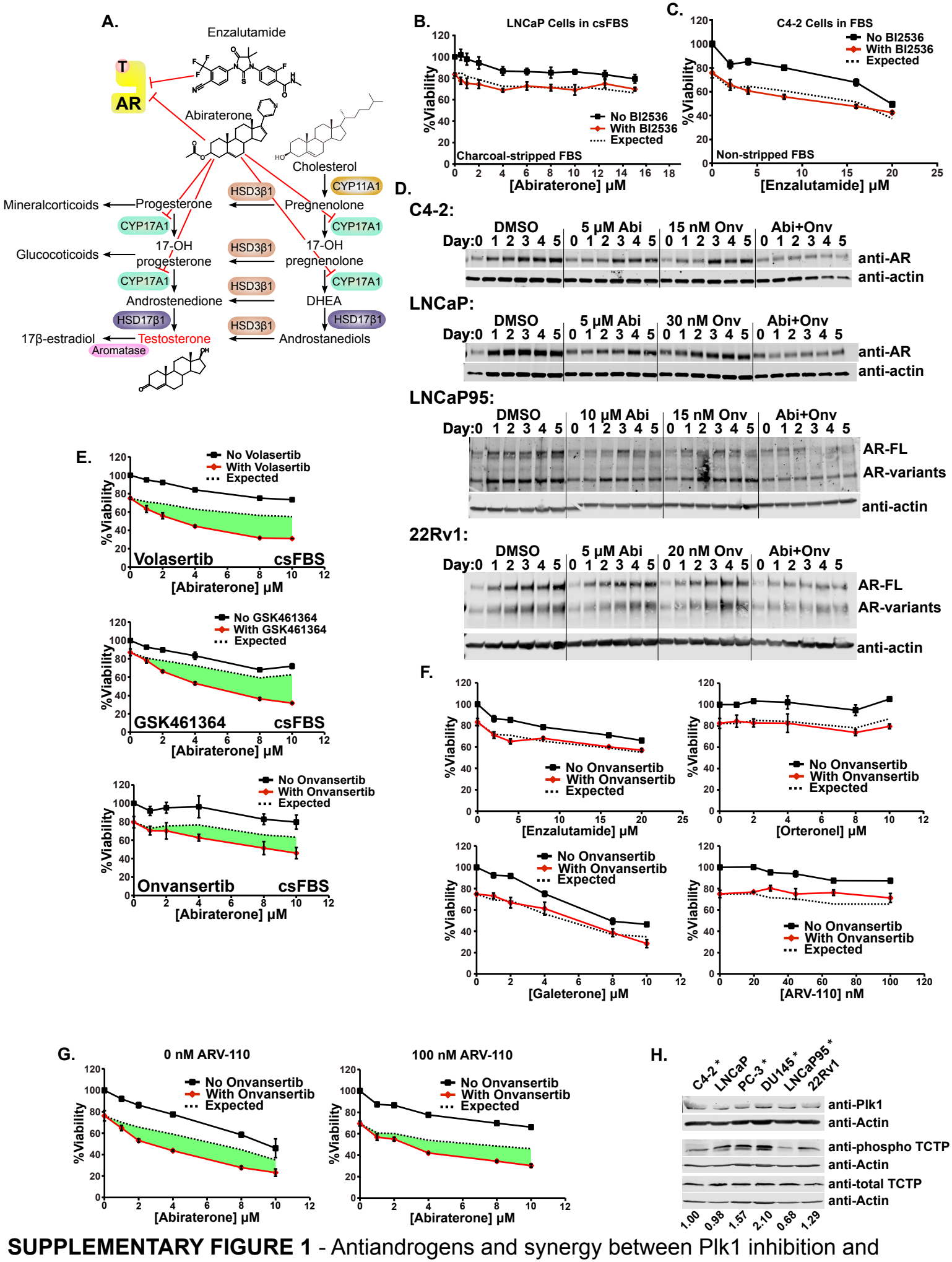

SUPPLEMENTARY FIGURE 1 - Antiandrogens and synergy between Plk1 inhibition and abiraterone

Supplementary Figure 1. Androgen signaling, antiandrogens, and synergy between Plk1 inhibition and abiraterone.

(A) Schematic of steroidogenesis and antiandrogen mechanism of action. Abiraterone inhibits Cyp17A1, an enzyme that catalyzes multiple steps in the conversion of cholesterol to testosterone. Both abiraterone and enzalutamide can directly inhibit the AR.

(B) Androgen-dependent LNCaP prostate cancer cells were grown in media containing csFBS and subjected to increasing concentrations of abiraterone in the presence (black lines) or absence (red lines) of BI2536 (10 nM). Viability relative to control at 72 hours was measured. Mean values ± SEM (n = 3) are shown. Expected viability (dotted black line) according to the Bliss independence model of drug additivity is plotted for comparison. Similar to **Fig. 1J** (cells grown in FBS). No synergy was seen in LNCaP cells in either medium.

(C) C4-2 CRPC cells were grown in media containing non-charcoal-stripped FBS and subjected to increasing concentrations of enzalutamide in the absence or presence of the Plk1 inhibitor BI2536 (2.5 nM). Synergy was assessed, analyzed and plotted as in (B). Similar to **Fig. 2C** (cells grown in csFBS), enzalutamide and Plk1 inhibitors do not synergistically kill C4-2 CPRC cells when grown in normal FBS.

(D) The indicated cell lines were treated with vehicle control, abiraterone, the Plk1 inhibitor onvansertib (here abbreviated Abi and Onv), or the combination and lysates collected at the indicated days. AR protein abundance was assessed by immunoblot with an antibody directed against the N-terminus of the AR. For lysates from LNCaP95 and 22Rv1 cells, the upper band is full-length AR (AR-FL), the lower band contains AR splice variants including AR-v7. While the combination of abiraterone and onvansertib does synergistically reduce AR and AR-v7 protein abundance, this occurs in all cell lines even though C4-2 and LNCaP95 were the only two that were synergistically killed by combined abiraterone and Plk1 inhibition.

(E) C4-2 CRPC cells were grown in media containing charcoal-stripped FBS and subjected to increasing concentrations of abiraterone in the absence or presence of volasertib (7.5 nM), GSK461364 (5 nM), or onvansertib (15 nM). Relative viability was assessed and plotted as in (B). Similar to **Fig. 2M**. Multiple distinct Plk1 inhibitors synergize with abiraterone in C4-2 CRPC cells regardless of the presence or absence of androgens.

(F) C4-2 CRPC cells were grown media containing FBS and subjected to increasing concentrations of the indicated antiandrogens in the presence or absence of the Plk1 inhibitor onvansertib. Synergy was assessed, analyzed, and plotted as in (B). Similar to **Fig. 2C-F**, but using onvansertib instead of

BI2536.

(G) C4-2 CRPC cells were subjected to increasing concentrations of abiraterone in the presence or absence of onvansertib (15 nM), without (left) or with (right) 100 nM of the AR-degrader ARV-110. Synergy was measured, analyzed, and plotted as in (B). Similar to **Fig. 2K**, but using onvansertib instead of BI2536.

(H) Immunoblots using lysates from the indicated cell lines assessing Plk1 abundance and activity. Cancer cell lines that showed synergistic killing to combined abiraterone-Plk1 inhibitor treatment are marked by '*'. Phosphorylation of serine 46 on TCTP was used as a measure of Plk1 kinase activity. Numbers at the bottom are phospho-TCTP over total TCTP (each normalized to their respective actin loading controls) relative to the TCTP phosphorylation observed in C4-2 cells. There is no correspondence of Plk1 protein abundance or activity with a synergistic response to the combination of abiraterone and Plk1 inhibition.

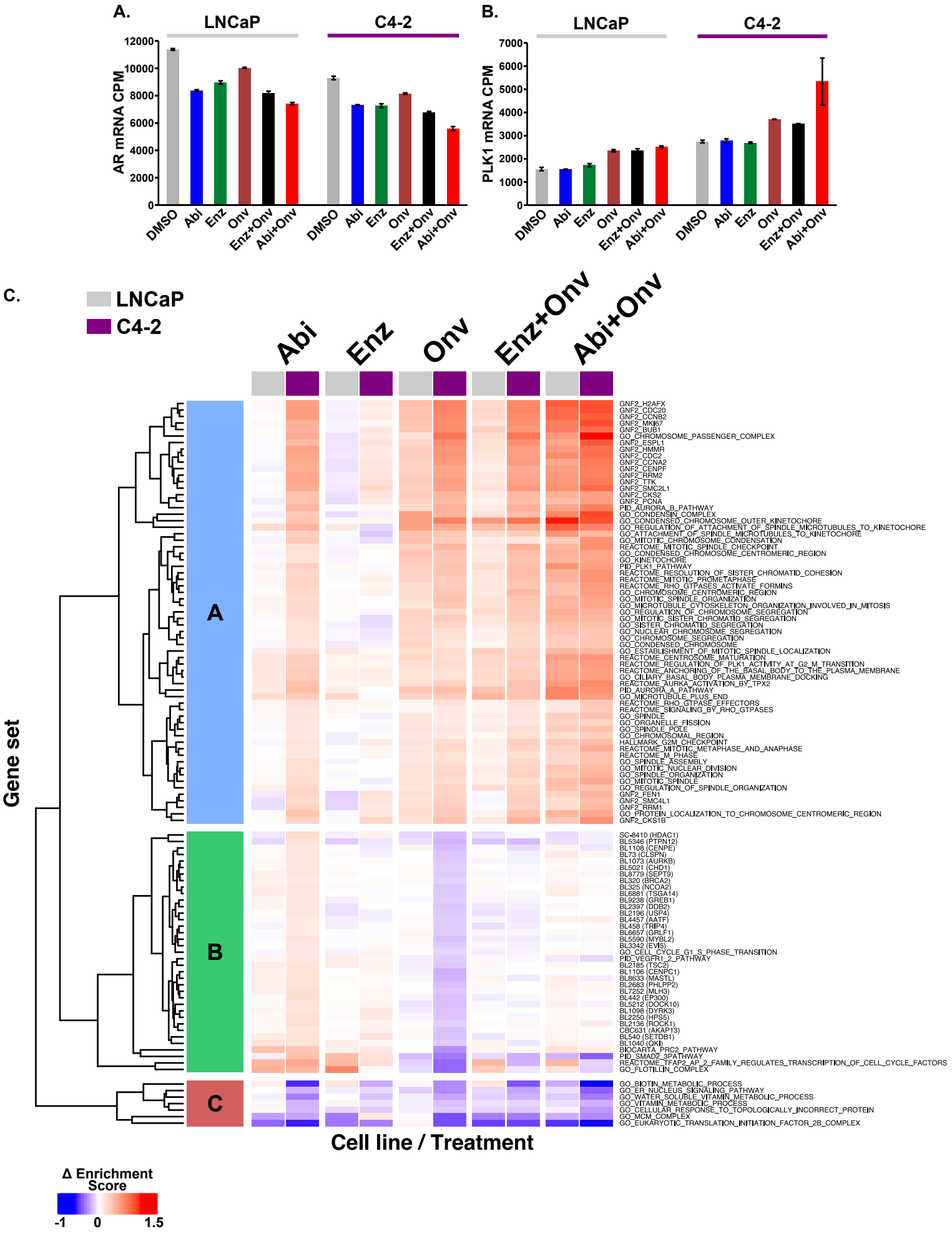

SUPPLEMENTARY FIGURE 2 - Abiraterone- and synergy-specific gene set signature identified from RNA sequencing analysis of prostate cancer cells.

Supplementary Figure 2. Abiraterone- and synergy-specific gene set signature identified from RNA sequencing analysis of prostate cancer cells.

(A) AR transcript levels measured in the RNA sequencing experiment described in **Fig. 3** in C4-2 and LNCaP cells after treatment with the indicated drugs.

(B) Plk1 transcript levels measured in the RNA sequencing experiment described in **Fig. 3** in C4-2 and LNCaP cells after treatment with the indicated drugs.

(C) Expanded and labeled version of the 109 gene set signature also shown in the **Fig. 3F** heatmap. The expression of these gene sets was significantly altered by both abiraterone and onvansertib only in C4-2 cells and not in LNCaP cells. The majority of the gene sets in Cluster A refer to cellular components, biological processes and gene neighborhoods that are related to mitosis and mitotic spindle assembly. It is noteworthy that they are upregulated by abiraterone but not enzalutamide treatment in C4-2 cells, and neither antiandrogen increases their expression in LNCaP cells.

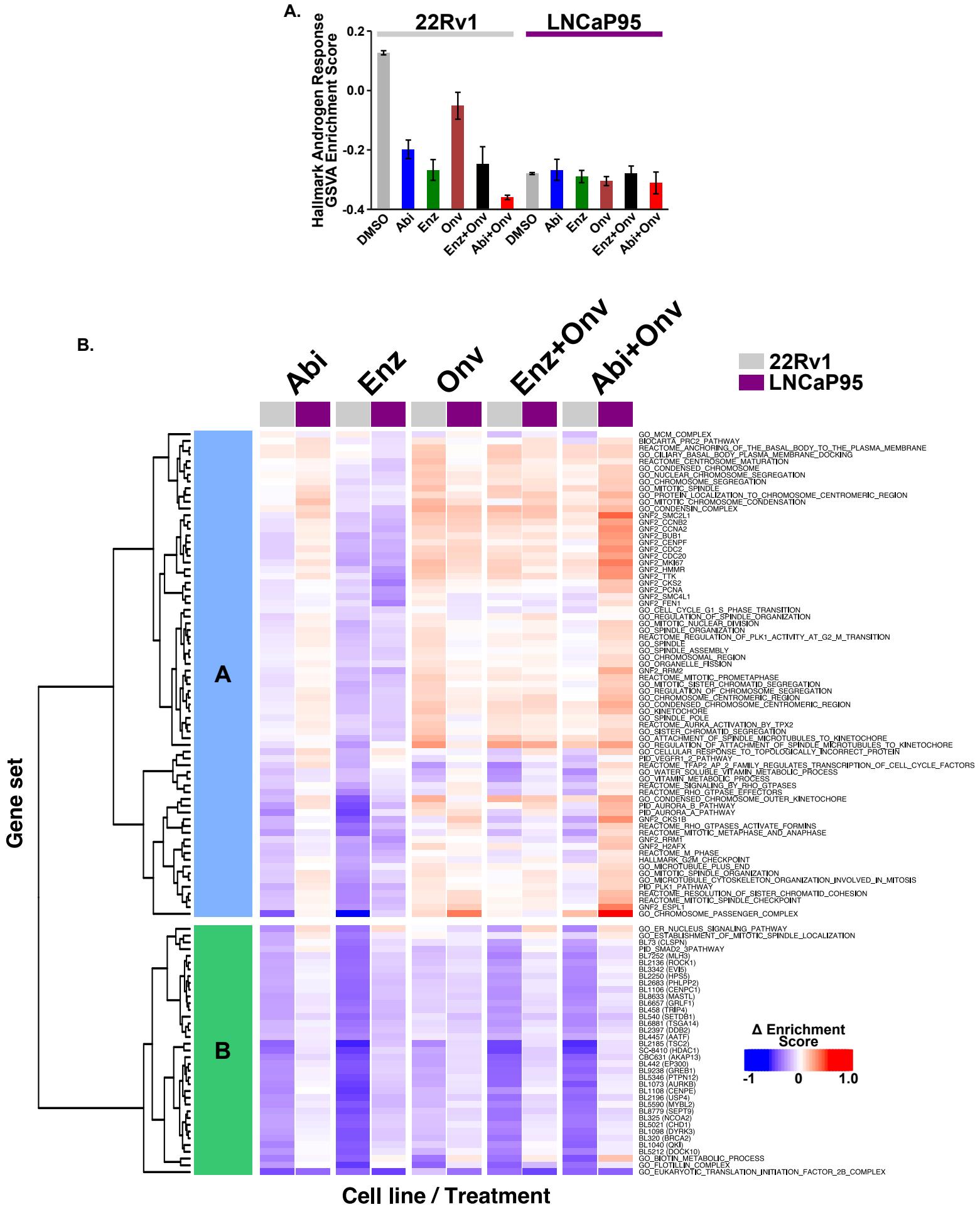

SUPPLEMENTARY FIGURE 3 - RNA sequencing analysis of additional prostate cancer cell lines confirms abiraterone- and synergy-specific gene set signature

Supplementary Figure 3. RNA sequencing analysis of additional prostate cancer cell lines confirms abiraterone- and synergy-specific mitotic gene set signature

(A) AR-dependent transcription in 22Rv1 and LNCaP95 AR-v7+ CRPC cells was examined using the Hallmark Androgen Response gene set in mSigDB after GSVA analysis. Bars indicate mean ± SEM. In 22Rv1 cells, which did not respond synergistically to combined abiraterone-Plk1 inhibitor treatment, AR-dependent transcription was moderately repressed by both antiandrogens and onvansertib. Combined abiraterone-onvansertib treatment suppressed the Androgen Response gene set even further. AR-dependent transcription in the synergistic LNCaP95 cell line was essentially unchanged in any treatment condition. This is consistent with the the vast majority of AR-dependent transcription in LNCaP95 cells being driven by the antiandrogen resistant AR-v7 splice variant, and is inconsistent with the notion that abiraterone-Plk1 inhibitor synergy is due to suppressed AR activity.

(B) Related to **Fig. 3I**. LNCaP95 cells were treated with 10 μM abiraterone, 20 μM enzalutamide, 15 nM onvansertib, and the indicated combinations. 22Rv1 cells were treated with 5 μM abiraterone, 10 μM enzalutamide, 20 nM onvansertib, and the indicated combinations. After 16 hours RNA was extracted for sequencing and analysis in a manner identical to that used for the C4-2 and LNCaP analysis presented in **Fig. 3**. Shown is hierarchical clustering of Δ enrichment scores for 109 gene sets contained in the AR-independent synergy-specific signature derived in **Fig. 3C-H**. Cluster A, which contains primarily gene sets related to mitosis and the mitotic spindle, was used for comparisons in **Fig. 3I**. These gene sets are upregulated by abiraterone, but not enzalutamide, only in LNCaP95 cells (purple columns) that had a synergistic response and not 22Rv1 cells (grey columns) which did not show synergy to the combination of abiraterone and Plk1 inhibition.

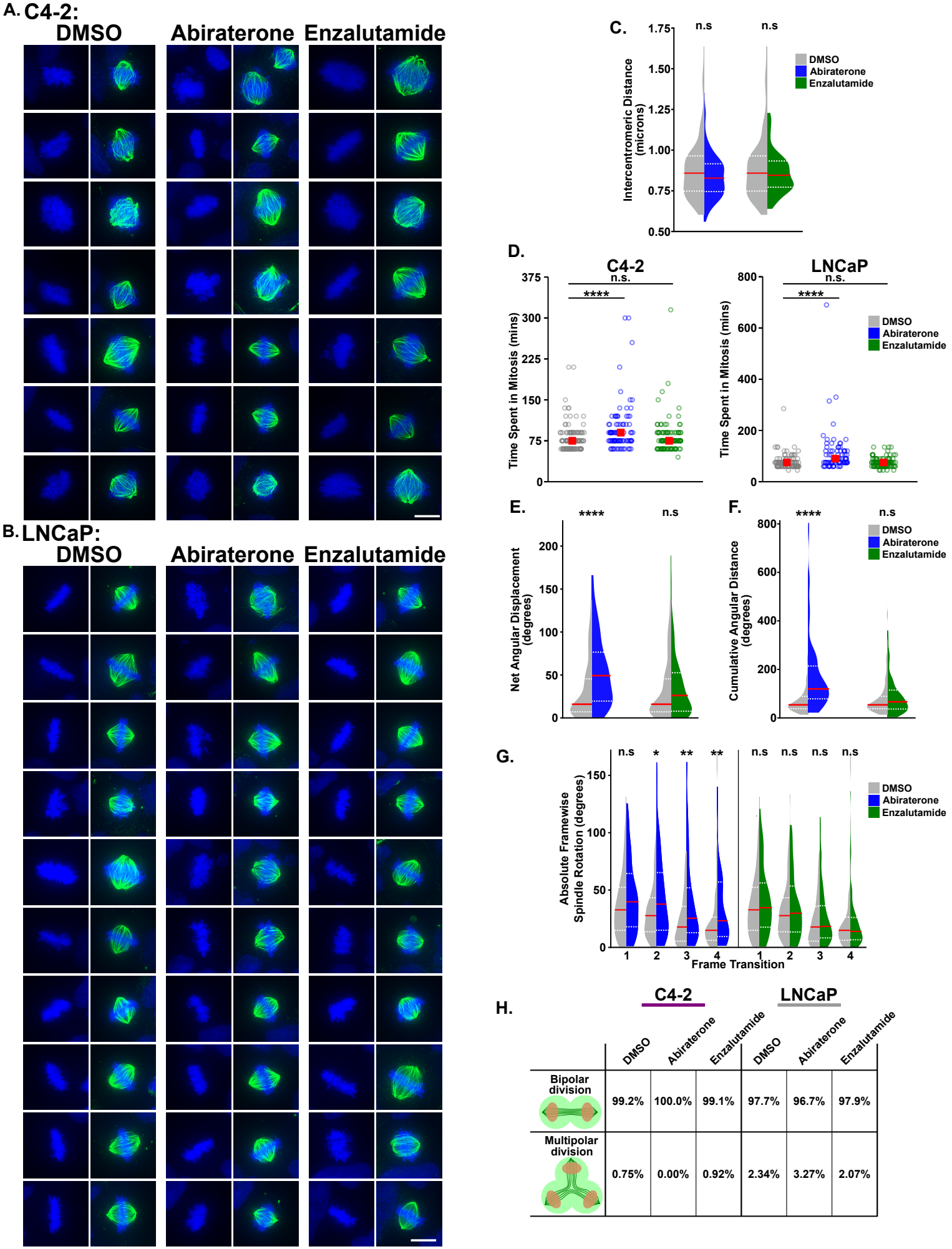

SUPPLEMENTARY FIGURE 4 - AR-independent effects of abiraterone on mitotic spindle assembly and chromatin condensation

Supplementary Figure 4. AR-independent effects of abiraterone on mitotic spindle assembly and chromatin condensation.

(A) Related to **Fig. 4A**. Seven additional examples mitotic spindle morphology in C4-2 cells after treatment with DMSO, abiraterone (5 μM), or enzalutamide (10 μM) for 24 hours. Fixed cells were stained with antibodies against tubulin (green) and DAPI for DNA visualization (blue). DMSO and enzalutamide treated cells had well-defined chromosome arms whereas abiraterone treated cells displayed ill-defined and apparently decondensed chromosome arms in mitotic cells. Scale bar lower right represents 10 μm.

(B) Micrographs of mitotic LNCaP cells treated DMSO, abiraterone (5 μM), or enzalutamide (10 μM) for 24 hours followed by fixation and staining with anti-tubulin antibodies (green) and DAPI (blue). Abiraterone treatment did not result in the appearance of decondensed mitotic chromosomes as judged by the similar size and definition of chromosome arms between the vehicle control and abiraterone treated LNCaP cells. Scale bar lower right represents 10 μm.

(C) LNCaP cells treated as in (B) were stained with antibodies against the centromeric histone CENP-A. Centromeres on sister chromatids were identified based on their paired orientation in three-dimensional space and microtubule fibers originating from opposite spindle poles. For an example in C4-2 cells see Supplementary Movie S4. Intercentromeric distance was measured between ten paired centromeres in ten cells per condition (n=100). Violin plots depicting the distribution of intercentromeric distances observed in DMSO, abiraterone, or enzalutamide treated cells. The red line represents the median and dotted white lines are upper and lower quartiles. n.s. not significant using a two-tailed Mann-Whitney U test.

(D) Related to **Fig. 4E**. C4-2 and LNCaP cells expressing H2B-mCherry and mEmerald-tubulin were grown in media containing FBS, subjected to vehicle control, abiraterone (5 μM), or enzalutamide (10 μM), and then analyzed by time-lapse live-cell microscopy. The duration of mitosis for individual cells was then determined by image analysis ($n \geq 86$). **** $p \leq 0.0001$, n.s. not significant using a two-tailed Mann-Whitney U test.

(E, F) Live-cell microscopy of LNCaP cells expressing H2B-mCherry and mEmerald-tubulin was used to quantify spindle rotation during mitosis in an identical manner to the analysis of C4-2 cells shown in **Fig. 4E-H**. Cells were treated with vehicle control, 5 μM abiraterone, or 10 μM enzalutamide, and imaged every 15 minutes for 72 hours. Shown are violin plots comparing the distribution of net angular displacement and cumulative angular distance in DMSO versus abiraterone or enzalutamide treated cells. The red line represents the median and dotted white lines are upper and lower quartiles ($n \geq 86$).

**** $p \leq 0.0001$, n.s. not significant using a two-tailed Mann-Whitney U test.

(G) The distribution of absolute rotations between frames during mitotic progression, where frame transition one represents the amount of spindle rotation between when a mitotic spindle was first apparent to the second frame. On the left are violin plots comparing vehicle control to abiraterone, on the right is the same comparison with enzalutamide. The red line represents the median and dotted white lines are upper and lower quartiles. * $p \leq 0.05$, ** $p \leq 0.01$, n.s. not significant using a two-tailed Mann-Whitney U test.

(H) The frequency of bipolar and multipolar spindle assembly and division in C4-2 and LNCaP cells treated as in (B). Neither abiraterone or enzalutamide increased the frequency of multipolar spindle formation in C4-2 or LNCaP cells ($n \geq 109$).

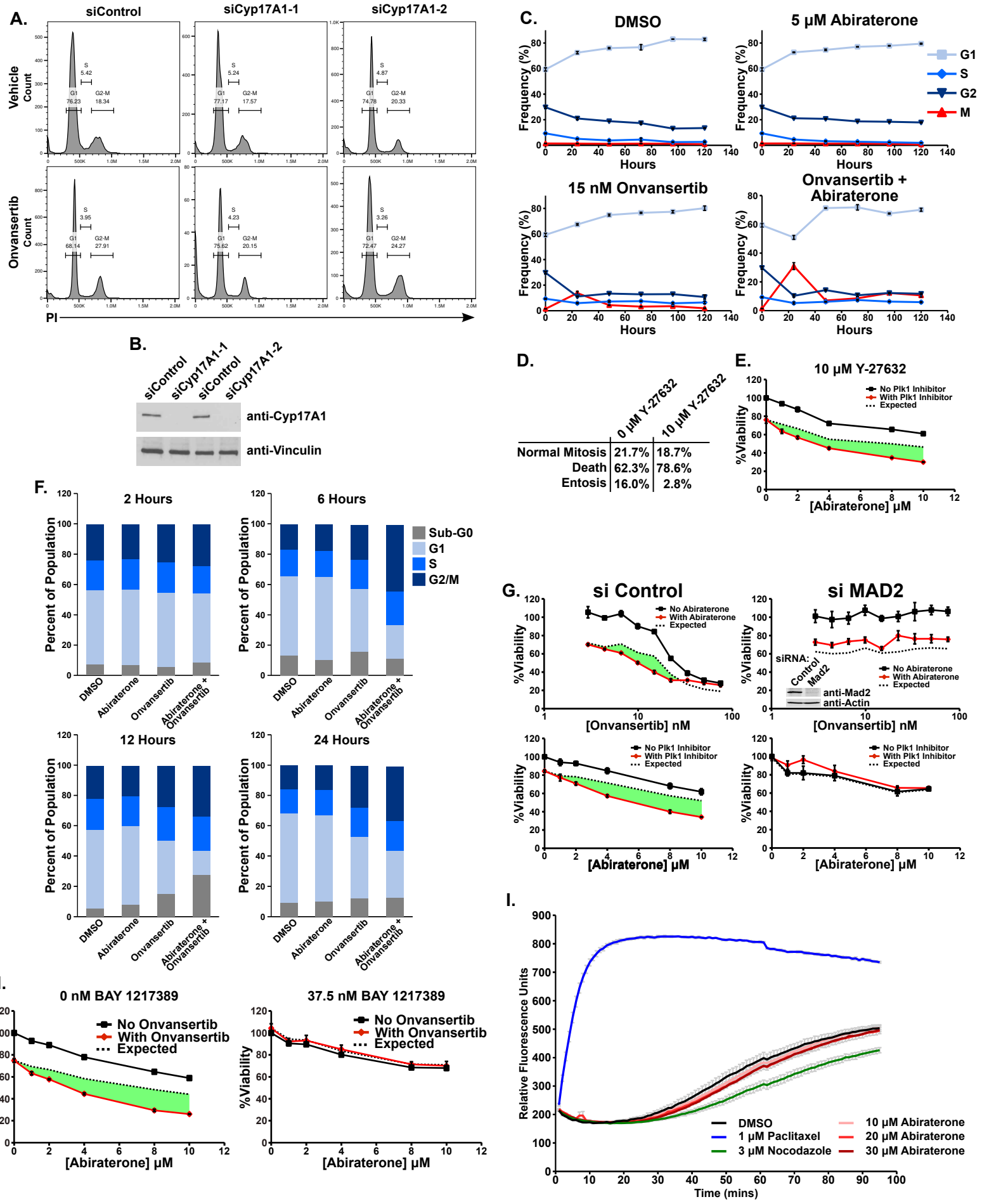

SUPPLEMENTARY FIGURE 5 - AR- and androgen-independent effects of abiraterone, onvansertib, and the combination on mitosis and cell cycle distribution in prostate cancer cells

Supplementary Figure 5. AR- and androgen-independent effects of abiraterone, onvansertib, and the combination on mitosis and cell cycle distribution in prostate cancer cells.

(A) C4-2 CRPC cells were transiently transfected with a control siRNA or one of two Cyp17A1-targeting siRNAs for 72 hours, and then subjected to 20 nM onvansertib for 6 hours prior to fixation. Cell cycle position was determined by flow cytometry using propidium iodide staining for DNA content. Shown are histograms depicting the distribution of DNA content. Gating was performed to separate G1, S and G2-M cells and their relative frequency among those gates is provided.

(B) Immunoblot confirmation of Cyp17A1 knockdown in C4-2 cells 72 hours after siRNA transfection.

(C) These data are related to **Fig. 5D**, in which we analyzed the percentage of mitotic C4-2 CRPC cells over a time course after treatment with abiraterone, onvansertib, and the combination. Cells were collected, fixed stained with DAPI and antibodies raised against pHH3, and then analyzed by flow cytometry. Mean ± SEM (n = 3). In **Fig. 5D**, we display only the percent mitotic. Here we provide percent G1, S, G2, and M phase cells over time in the four conditions.

(D) C4-2 cells expressing H2B-mCherry and mEmerald-tubulin were used for live-cell microscopy in an identical manner as presented in **Fig. 4E**. The frequencies of normal cell division, cell death in or shortly after mitosis, and entotic cell death were tracked in cells treated with abiraterone (5 μM) and onvansertib (15 nM) with or without 10 μM Y-27632 an inhibitor of Rock1. Rock1 inhibition dramatically reduced, but did not eliminate, entosis after cotreatment with abiraterone and onvansertib. The overall amount of cancer cell death was unchanged.

(E) Synergy between abiraterone and onvansertib was assessed in the presence of 10 μM Y-27632 Rock1 inhibitor. C4-2 cells were treated with increasing concentrations of abiraterone in the presence (red line) or absence (black line) of 15 nM onvansertib. Shown is viability relative to control 72 hours after drug addition, mean ± SEM (n = 3). The dotted black line represents the expected response based on the Bliss independence model of drug additivity. Inhibition of Rock1, and subsequent loss of entosis, did not eliminate they synergistic cancer cell killing achieved by combined abiraterone and onvansertib.

(F) DU145 AR-negative prostate cancer cells were treated with DMSO, 10 μM abiraterone, 10 nM onvansertib, or the combination for the indicated time prior to fixation. Cells were then stained with propidium iodide and their DNA content analyzed by flow cytometry as an indicator of cell cycle position.

(G) Related to **Fig. 5I**. An additional MAD2-targeting siRNA was used to disable the SAC and assess synergy between abiraterone and onvansertib. C4-2 cells were transfected with a control siRNA (N1,

left panels) or an siRNA targeting MAD2 (right panels). Thermo Fisher *Silencer*® Select siRNAs targeting different exons of MAD2 s8392 and s8393 were used in **Fig. 5I** and here, respectively. After 24 hours the cells were replated, and the following day subjected to increasing concentrations of onvansertib in the presence of 8 μM abiraterone (top) and increasing concentrations of abiraterone in the presence of 15 nM onvansertib (bottom). Data were acquired, analyzed and plotted as in (E). The immunoblot inset in the upper right panel confirmed Mad2 knockdown 48 hours after siRNA transfection.

(H) C4-2 cells were treated with increasing concentrations of abiraterone with or without 15 nM onvansertib in the absence (left) or presence (right) of 37.5 nM of the MPS1 inhibitor BAY 1217389. After 72 hours synergy was assessed and analyzed and plotted as in (E). MPS1 is a dual-specificity kinase whose activity is required for recruitment of SAC components to kinetochores. Loss of SAC activity through MPS1 inhibition abrogated synergy between abiraterone and onvansertib.

(I) Purified α/β-tubulin was polymerized into microtubules by incubation at 37°C and addition of 1 mM GTP in the presence of microtubule stabilizing drug paclitaxel, a microtubule polymerization inhibitor nocodazole, or the indicated doses of abiraterone. Tubulin polymerization was measured over the course of 100 minutes using DAPI which displays enhanced fluorescence upon binding to polymerized microtubules. Mean ± SEM (n = 3).

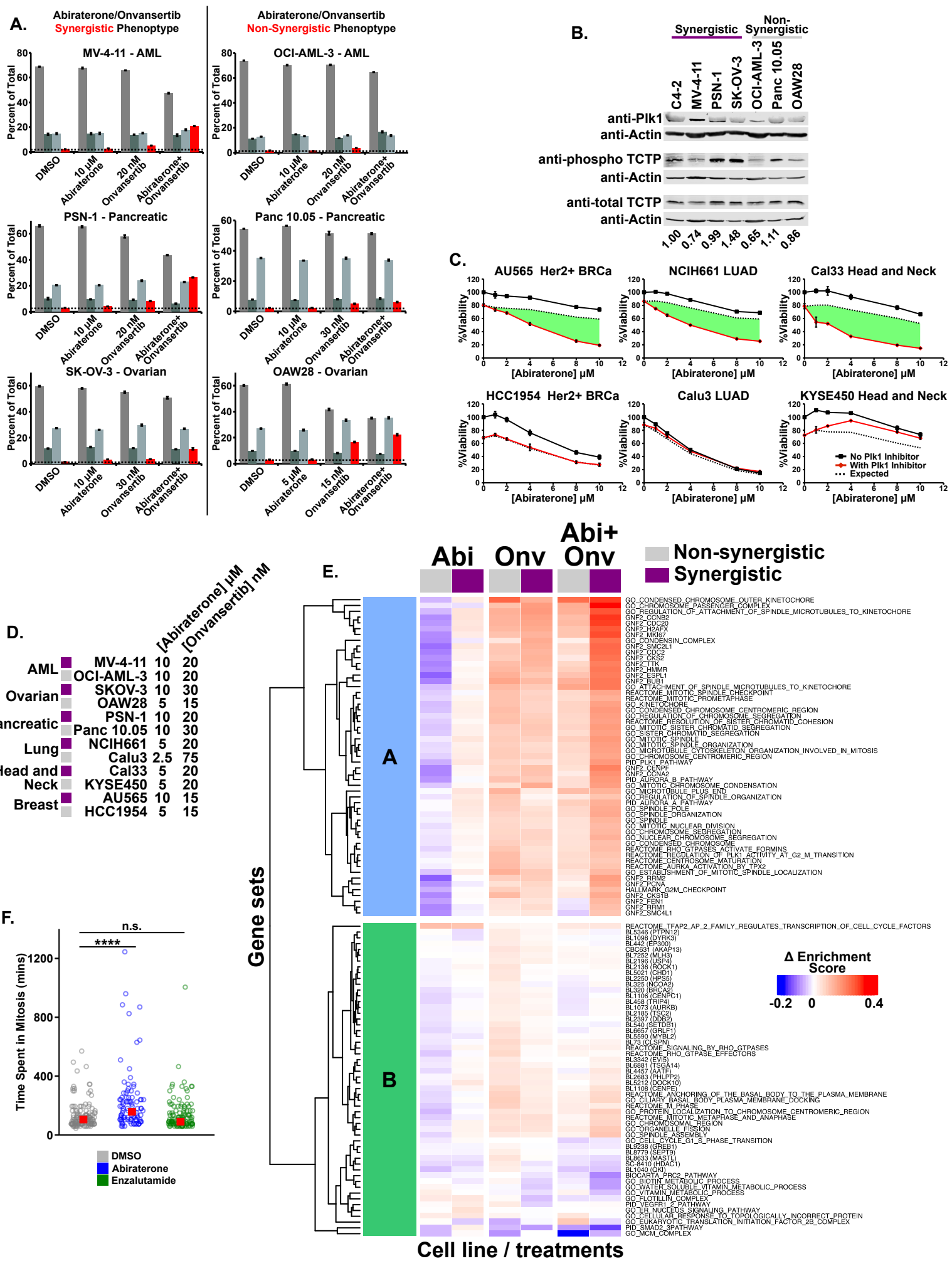

SUPPLEMENTARY FIGURE 6 - Effects of abiraterone, onvansertib, and the combination on AR-negative non-prostate cancer cells

Supplementary Figure 6. Effects of abiraterone, onvansertib, and the combination on AR-negative non-prostate cancer cells.

(A) These data are related to **Fig. 6C**. The indicated cell lines were treated with the indicated drugs for 16 hours, fixed and then stained with DAPI and antibodies against pHH3 to assess cell-cycle distribution by flow cytometry. These graphs show the percentage of cells in each stage of the cell cycle in addition to the percentage of cells in mitosis presented in **Fig. 6C**. Abiraterone treatment was 10 μM for all cell lines except OAW28, which was 5 μM. Onvansertib concentrations used were 20 nM for MV-4-11, OCI-AML-3, and PSN-1; 30 nM for Panc 10.05 and SK-OV-3; 15 nM for OAW28. Mean ± SEM (n = 3).

(B) Measurement of Plk1 protein abundance and activity in lysates from the indicated cancer cell lines. The first four cell lines respond synergistically to the combination of abiraterone and onvansertib, whereas the last three do not. Plk1 kinase activity was assessed by detecting phosphorylation of serine 46 on TCTP. Numbers at the bottom are phospho-TCTP over total TCTP (each normalized to their respective actin loading controls) relative to the TCTP phosphorylation observed in C4-2 cells. There is no correspondence of Plk1 protein abundance or activity with a synergistic response to the combination of abiraterone and Plk1 inhibition.

(C) Related to **Fig. 6E-H**. Six additional non-prostate cancer cell lines from three other tumor types used for RNA sequencing analysis. Three of these cell lines have synergistic responses to the combination of abiraterone and onvansertib and three do not. Each cell line was subjected to increasing concentrations of abiraterone in the absence (black lines) or presence (red lines) of onvansertib (AU565 15 nM, HCC1954 15 nM, NCIH661 22.2 nM, Calu3 75 nM, Cal33 22.2 nM, and KYSE450 15 nM). Viability relative to control was measured after 72 hours (mean ± SEM, n = 3). The dotted line represents expected combined result according to the Bliss independence model of drug additivity and the areas shaded in green indicate synergy.

(D) Doses of abiraterone and onvansertib used for RNA sequencing analysis of a panel of 12 non-prostate cancer cell lines. Cell lines that responded synergistically and those that did not are indicated by purple and grey boxes, respectively, and are paired by indication.

(E) Related to **Fig. 6F**. Expanded and labeled version of the AR-independent synergy-specific 109 gene set signature expression in the non-prostate cancer cell line RNA sequencing analysis. Values represent mean Δ enrichment scores among synergistic or non-synergistic cancer cell indicated by purple and grey boxes, respectively. Unsupervised hierarchical clustering identified two clusters. Cluster A contains gene sets whose function are strongly associated with mitosis and the mitotic spindle. These

gene sets are upregulated by abiraterone and are induced synergistically by the combination only in AR-negative non-prostate cancer cells that were synergistically killed by combined abiraterone and onvansertib.

(F) Related to **Fig. 6I**. SK-OV-3 cells expressing H2B-mCherry and mEmerald-tubulin were subjected to vehicle control, abiraterone (10 μM), or enzalutamide (20 μM), and then analyzed by time-lapse live-cell microscopy. The duration of mitosis for individual cells was then determined by image analysis ($n \geq 143$). **** $p \leq 0.0001$, n.s. not significant using a two-tailed Mann-Whitney U test.

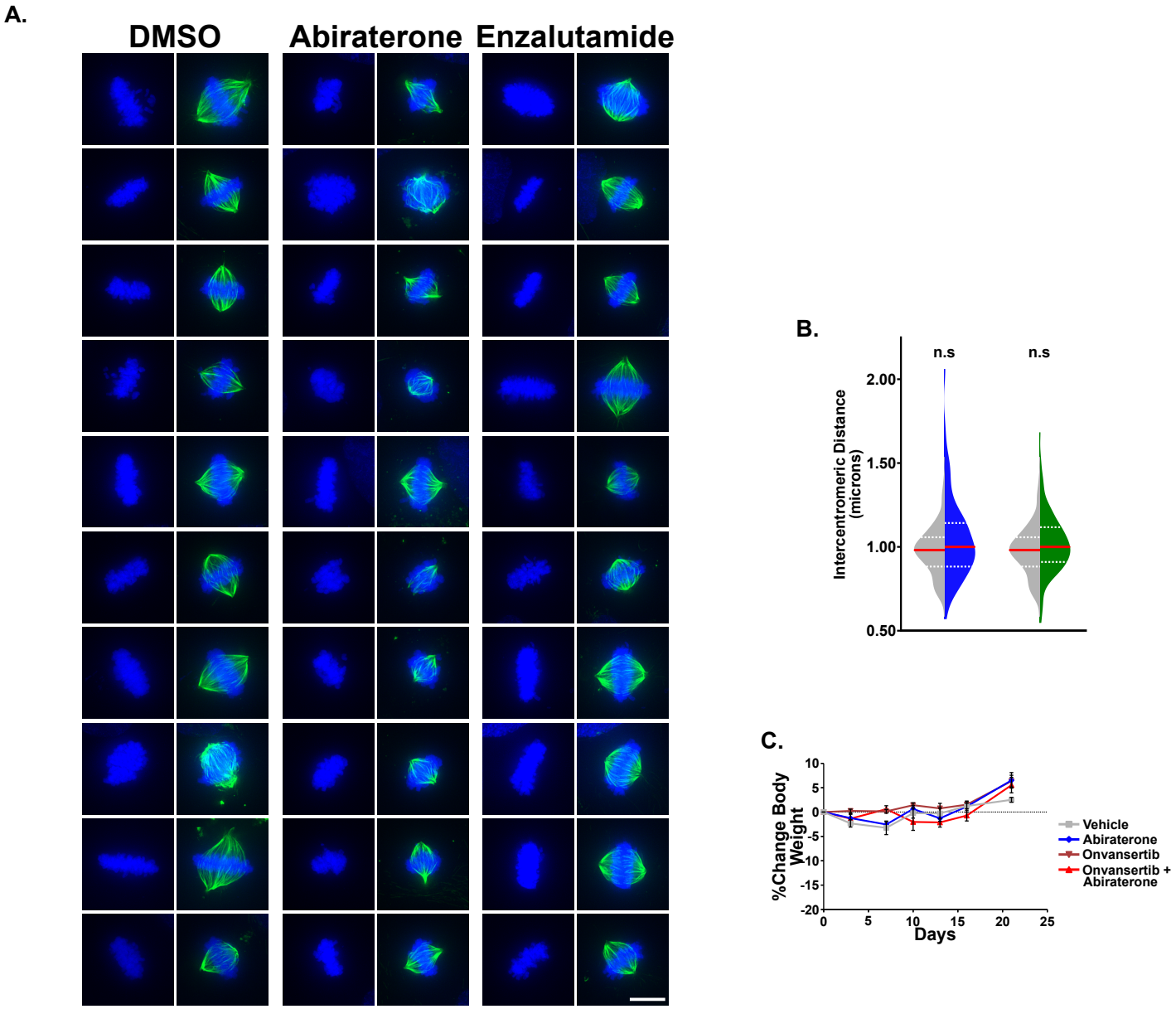

SUPPLEMENTARY FIGURE 7 - Analysis of abiraterone-dependent mitotic defects in SK-OV-3 cells, and mouse weights from *in vivo* study

Supplementary Figure 7. Analysis of abiraterone-dependent mitotic defects in SK-OV-3 cells, and mouse weights from the *in vivo* study

(A) SK-OV-3 ovarian cancer cells were treated with vehicle control, 10 μM abiraterone, or 20 μM enzalutamide for 24 hours, fixed and stained with DAPI (blue) and anti-tubulin antibodies (green). Unlike C4-2 CRPC cells, abiraterone treatment did not cause obvious defects in chromatin condensation as chromosome arm size and overall metaphase plate structure are similar between DMSO, abiraterone and enzalutamide treated cells. Scale bar lower right represents 10 μm.

(B) SK-OV-3 cells treated as in (A) were additionally stained with anti-CENP-A antibodies. As done using C4-2 cells in **Fig. 4C** and shown in Supplementary Movie S4, centromeres on sister chromatids were identified, and intercentromeric distance was measured between ten paired centromeres in ten cells per condition (n=100). Violin plots depicting the distribution of intercentromeric distances observed after DMSO, abiraterone, or enzalutamide treatment. The red line represents the median and dotted white lines are upper and lower quartiles; n.s. not significant using a two-tailed Mann-Whitney U test.

(C) These data are related to **Fig. 7A**. Body weights of mice treated with the indicated drugs or combination over time. Mean ± SEM is shown.

SUPPLEMENTARY MATERIALS

Supplementary Movie S1. Chromatin structure in vehicle treated C4-2 cells

Supplementary Movie S2. Chromatin structure in abiraterone treated C4-2 cells

Supplementary Movie S3. Chromatin structure in enzalutamide treated C4-2 cells

Supplementary Movie S4. Identification of paired centromeres from sister chromatids

Supplementary Movie S5. Video montage comparing mitosis of vehicle control with abiraterone treated C4-2 cells

Supplementary Movie S6. Normal mitotic cell division

Supplementary Movie S7. Cellular division that occurred in a manner that was not parallel to the growth surface

Supplementary Movie S8. Example of mitotic arrest and cell death caused by abiraterone and onvansertib

Supplementary Movie S9. Entosis of mitotic C4-2 cells